buildings

MDPI

Article

Investigation and Analysis of Stress and Deformation Monitoring of Long-Span Steel Roof Trusses

Cun Hui [1,*], Yongkang Jiao [1], Mingliang Liu [2,3] and Ran Hai [1,*]

[1] School of Architecture and Civil Engineering, Zhongyuan University of Technology, Zhengzhou 450007, China
[2] School of Civil Engineering, Chang'an University, Xi'an 710061, China
[3] Shaanxi Academy of Building Research Co., Ltd., Xi'an 710082, China
* Correspondence: hcun@zut.edu.cn (C.H.); lilihai2001@163.com (R.H.); Tel.: +86-13526592880 (C.H.)

Abstract: Structural stress and deformation monitoring and analysis were carried out for the 54 m long-span steel roof truss. To ensure the safety of the construction process, the stress and deformation of the steel roof trusses were monitored throughout the construction process. The numerical modeling of the structures with six different working conditions was carried out, and the points with the most critical values of stress and deformation were found. This work provides a theoretical basis for field monitoring during and after construction. The results show that the maximum vertical displacement of a steel roof truss during all modeled working conditions and the maximum measured displacement are within the Chinese building code's requirements. The maximum value of stress found during analysis of the structure during the construction process and the maximum measured stress are much less than the yield stress. The structural stress remains in the elastic range. The reasons for the differences between the calculated and measured results were analyzed.

Keywords: steel roof truss; long-span; stress and deformation; health monitoring; numerical simulation

Citation: Hui, C.; Jiao, Y.; Liu, M.; Hai, R. Investigation and Analysis of Stress and Deformation Monitoring of Long-Span Steel Roof Trusses. *Buildings* **2023**, *13*, 398. https://doi.org/10.3390/buildings13020398

Academic Editor: André Rafael Dias Martins

Received: 3 January 2023
Revised: 10 January 2023
Accepted: 19 January 2023
Published: 1 February 2023

1. Introduction

With the continuous development of the Chinese construction industry, long-span truss structures have become more widely used in recent years. In order to ensure the reliability and safety of long-span truss structures, simulation and other analysis techniques are important for understanding the stress and deformation of the structures before construction. Therefore, structural modeling and analysis of long-span truss structures has become an important research branch of structural engineering. Meanwhile, the health monitoring of the long-span structures is much more important for the construction process, especially the stress and deformation. Based on the key parameters of five structures and finite element models, Zhang et al. [1] proposed a general method for forming models of super-long-span latticed shells and determining the stresses seen in megalatticed shells under static loads. Su et al. [2] summarized the principles and empirical formulas of background and resonance factors, providing a theoretical basis for engineers to better understand wind-induced vibration effects in long-span roof structures. Dong et al. [3] described the characteristics of spatial structures and their application and development in China. Chen et al. [4] described the detailed steps for a design response spectrum and verified its feasibility through an example of the vertical vibration of a long-span structure. Chen et al. [5] carried out numerical simulations and analyses to compare the surface wind pressure and vibration characteristics of straw-hat long-span spatial structures and systematically studied the influence of key parameters, such as their height-span ratio on the distribution of wind pressure at different parts of straw-hat structure surfaces. Li et al. [6] used the large eddy simulation method to study the unsteady aerodynamic characteristics of long-span roofs. Their results showed that the displacement

responses of structures are underestimated if unsteady aerodynamic effects are not considered. Wang et al. [7] validated the feasibility of an improved method based on a Bayesian dynamic linear model, using real-time monitoring data from a long-span cable-stayed bridge. Liang et al. [8] studied characteristics and control measures for the structural noise of long-span steel truss cable-stayed bridges designed for urban rail transit systems. Diana et al. [9] outlined the wind tunnel activities and methods developed in recent years to support the design of long-span suspension bridges and proposed a method combining results from numerical and experimental methods. Lee et al. [10] adapted the four-node Lagrange finite element method and the Helmite finite element method to carry out three-dimensional dynamic analysis of long-span box girder bridges with moving loads. Their results showed that the dynamic effects of different sections and locations, which mainly manage the behavior of box girder structures subjected to dynamic loads, should not be ignored. Kim et al. [11] designed a practical wireless sensor network system and carried out real-time structural health monitoring for the large-span main girder of a building under construction. Chen et al. [12] proposed an improved physical theory model and tested it to prove its validity. Feng et al. [13] used finite element analysis to determine the most-stressed cable and its stress amplitude. Santana et al. [14] studied the nonlinear behavior of conical space trusses under vertical and horizontal loads by using the finite element models, considering the constitutive relations of large displacements and rotations, geometric imperfections, and elastic–plastic materials. They also examined the influences of geometric parameters on the bistable performance and load-bearing capacity of roofs. Feng et al. [15] studied the yield behavior of core truss members and the elastic buckling and yield behavior of panel members. Zhu et al. [16] proposed a framework to analyze stress levels due to buffeting for double-box cable-stayed bridges seeing distributed wind loads. Mahmoud et al. [17] carried out a three-dimensional nonlinear dynamic analysis using finite element simulation and studied the potential for failure of steel structures and braced steel frames under earthquake-induced loads. Research on parametric vibration of a steel truss corridor under pedestrian excitation considering the time delay effect was studied by Chen et al. [18]. The mechanical and creep properties [19], structural optimization [20], seismic isolation performance [21], and mechanical properties [22] are studied in these years.

According to the specifications [23–27], the stresses and deformations of the eighth of the steel trusses in the landing hall of the Xi'an Silk Road International Exhibition Center in China were analyzed using finite element models. The most critical points of stress and deformation were discovered and discussed. The measured strain and deformation of the long-span steel trusses fabricated during the construction process were compared with the results for those structures from finite element analysis to verify the validity of the finite element models. By comparing the measured and the calculated results for these stresses and deformations, the validity of the models and the safety and stability of the structure are evaluated.

2. Project Profile

The Xi'an Silk Road International Exhibition Center project is in the core of the Chanba ecological district of the city of Xi'an in China. As the center of China's national "The Belt and Road" construction, this project was expected to be a large-scale exhibition center, integrating exhibition areas, exchange areas, and trading areas. The main building includes functions to support exhibitions, commercial activities, catering, and parking. There are six single-layer pavilions (W1–W6) on the west side and six single-layer pavilions (E1–E6) on the east side. The 12 independent exhibition halls in the above-ground section are connected by the north–south entrance hall and the north–south connecting corridor. The planar projected area of the entrance hall on the south side is 144 m $\times$ 90 m. The height of the eaves just below the roof is 37 m. The maximum height of the roof is 37.75 m, and its maximum span is 54 m. The column spacing is 9 m.

The main structure of the main exhibition hall of the exhibition center is a reinforced concrete frame, and the roof is a tubular truss structure. The steel truss of the roof and the main structure are connected by aseismic hinge supports. The main structure of the landing hall is a reinforced concrete; the roof is a tubular truss structure, its span is 54 m, its maximum cantilever length is 18 m, the minimum height of the trusses is 2.5 m, and the truss maximum height is 4.5 m. The building plan is shown in Figure 1.

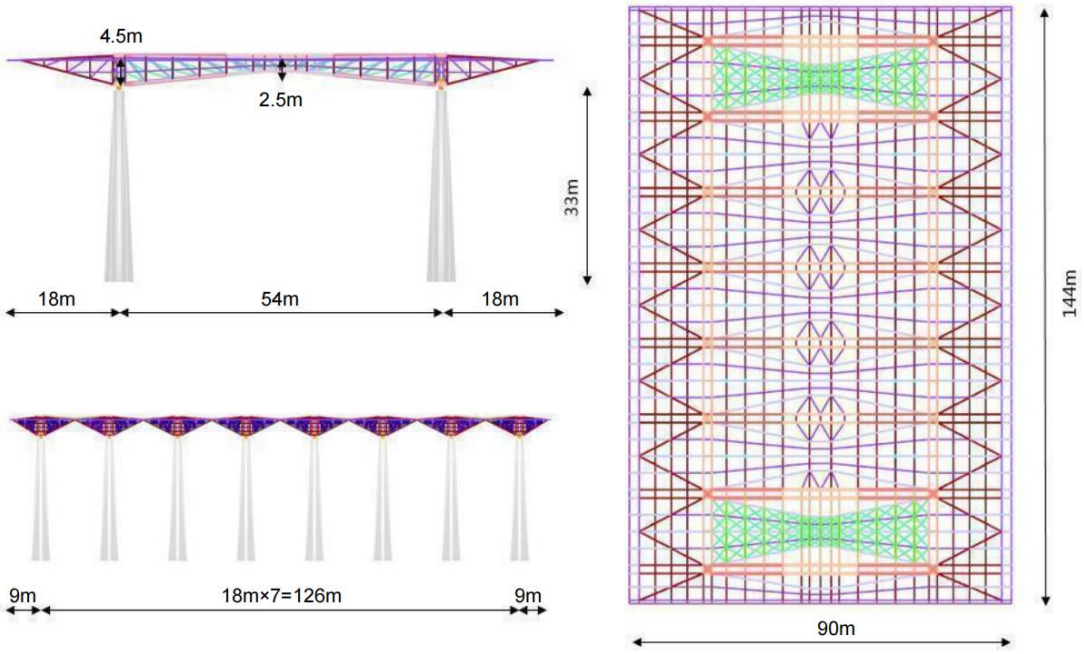

Figure 1. Architectural plan.

3. Engineering Structure Features

3.1. Complex Structural System

The roof structure of the landing hall uses tubular trusses, which take the form of a flat upper section and a folding lower section. The two ends of each truss are supported on a concrete cross column and are connected to the concrete cross column through the spherical seismic bearing. All the tubular fittings of the truss are connected to another, and some of the rods at the joints are relatively close. The structure is complex. A typical model of the steel roof truss structure is shown in Figure 2.

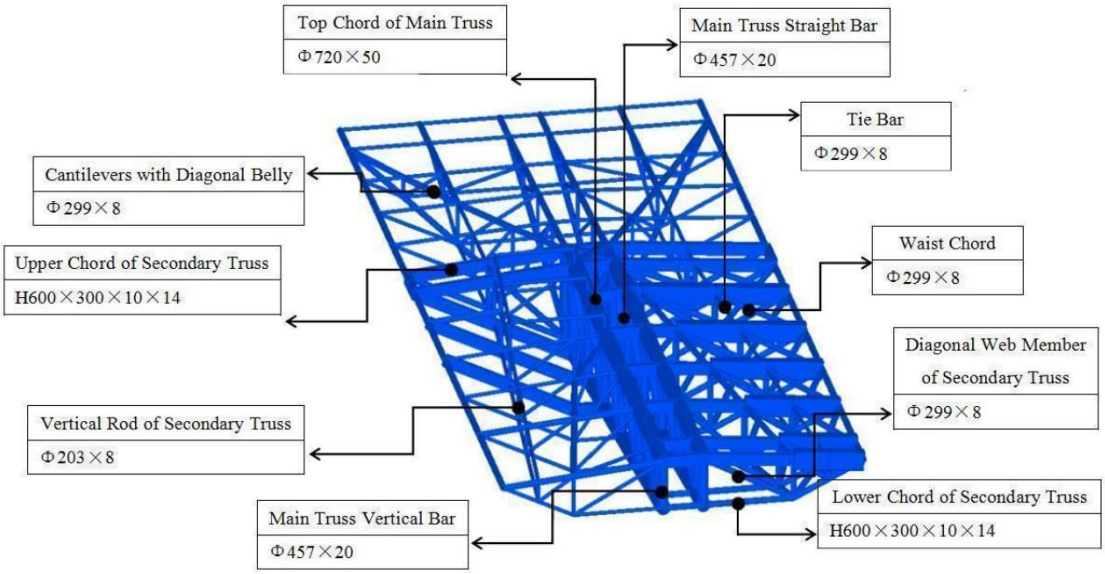

Figure 2. Model of the typical steel truss structure.

The length of the truss is 90 m, the span is 54 m, the maximum cantilever length is 18 m, the highest height of the roof is 37.75 m, the height of the support is 33 m, the minimum height of the truss is 2.5 m, and the maximum height is 4.5 m.

3.2. Complex Construction Process

The construction process for the landing hall involves joining together and hoisting two main assemblies. The construction process has a great deal of impact on the overall stress and deformation of the structure. The unforeseeable variables in the construction process, if not monitored and controlled, will affect the construction process and the safety of the structure after its completion. Two 250 t crawler cranes are used to lift the main truss. At the same time, 50 t and 25 t truck cranes are used for assembling, unloading, and transferring smaller components. The main truss is lifted and put in place, and the crane hooks are loosened after the two ends are welded together and reinforced to ensure that the truss is part of a stable system.

To ensure that the installation progress goes smoothly and to reduce the time to assemble and weld the trusses, a large portion of the assembly and welding work is done in advance. During the construction of the reinforced concrete frame, the assembled trusses can be stored and prepared in advance for sliding and hoisting operations.

3.3. Difficulty to Monitor

Some of the required monitoring data are difficult to collect. This is due to the complexity of the exhibition center's steel roof truss structure, its large span, the wide monitoring coverage required, the poor conditions of measuring-point arrangements on the steel members, interference fields, the hidden locations of some monitored points, and also possible future requirements for sensor installation and monitoring needed when there is a significant security concern. In addition, the scaffolding needed during construction is not needed after construction is finished.

4. Finite Element Analysis

4.1. Model Development

In this paper, a three-dimensional finite element model was developed using the Sap 2000. The truss model was divided into 203 nodes and 285 beam elements. The eighth truss of the landing hall was chosen as the object of this analysis. It is shown in Figure 3. In the finite element model, all the element types are truss elements and they are

meshed automatically by the software. The columns are fixed with the ground, and three displacement components and three rotation components are set as zero.

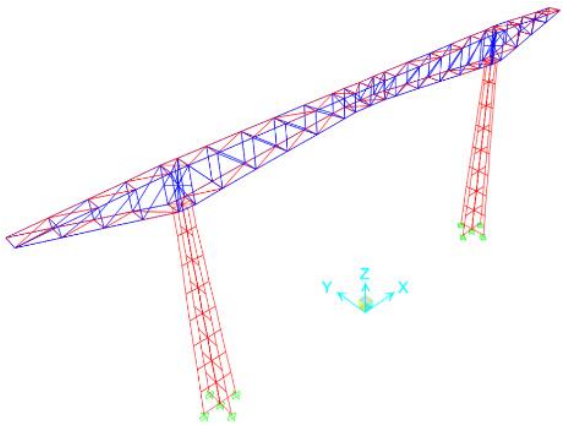

Figure 3. Finite element model of the eighth steel roof truss.

4.2. Material Characteristic Parameter

According to the relevant standard [23], the elastic modulus of structural steel E is 2.06×10^5 N/mm^2, the shear modulus G is 7.9×10^4 N/mm^2, the linear expansion coefficient α is $12 \times 10^{-6}/^{\circ}$C, and density ρ is 7850 kg/m^3. Only the constant load, live load, and the wind load in the X and Y directions are considered in this paper.

4.3. Interpretation of Results

According to the standard [23], the conditions are analyzed under different working conditions, including dead load (D), dead load + live load (D + L), dead load + live load + wind load (D + L + 0.6WX/Y), and the wind suction effect (0.7D + WX/Y). The label number for each working condition and the corresponding load on the truss are shown in Table 1. The dead load (D) is composed of the dead weight of the structure and the roof. The dead weight of the structure is automatically calculated and applied by the program. The live load (L) is the live load of the roofing equipment, and it is taken to be 7.0 kN/m^2. WX and WY are the wind loads in the X and Y directions, respectively. The stress and deformation of the structure under different load conditions are shown in Figures 4–9. In the deformation diagrams, (x, y, z) represent the deformation of the labeled point in the direction of x, y, and z (mm). In the stress diagram, (σ1, σ2) represent the maximum and minimum stresses (MPa). The results of this analysis are shown in Table 2.

Table 1. Load on the truss due to various working conditions.

Condition Number	Load Application
Condition 1	D
Condition 2	D + L
Condition 3	D + L + 0.6WX
Condition 4	D + L + 0.6WY
Condition 5	0.7D + WX
Condition 6	0.7D + WY

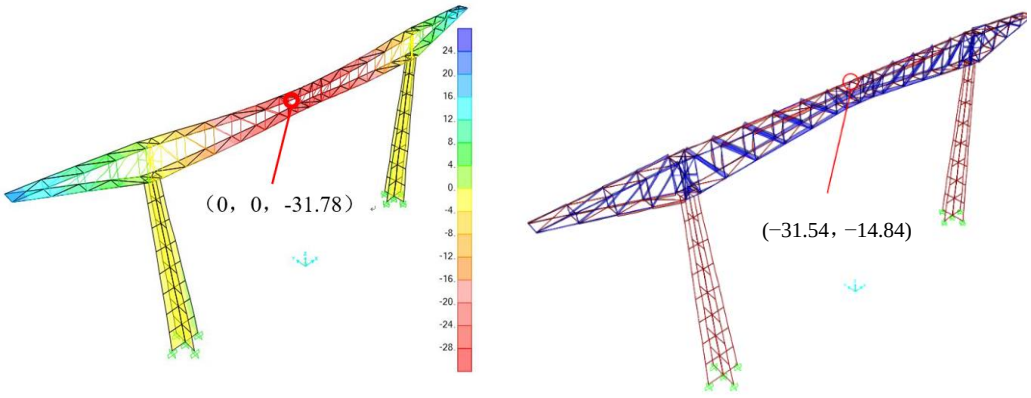

(**a**) (**b**)

Figure 4. Condition 1. (**a**) Deformation pattern. (**b**) Stress diagram.

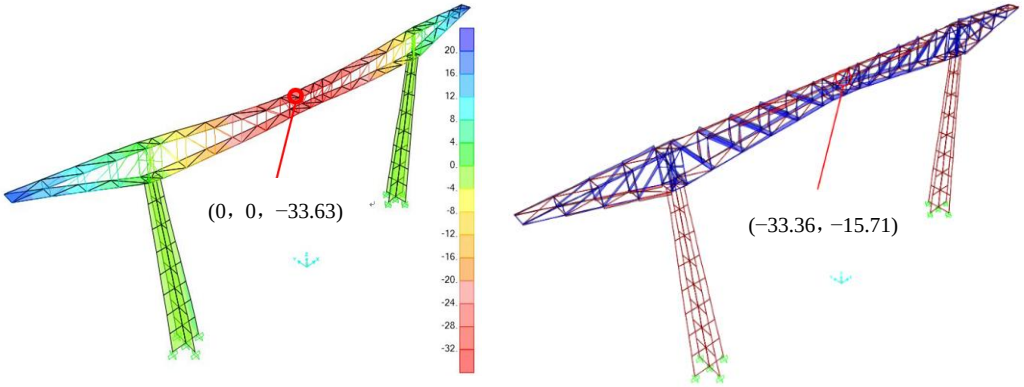

(**a**) (**b**)

Figure 5. Condition 2. (**a**) Deformation pattern. (**b**) Stress diagram.

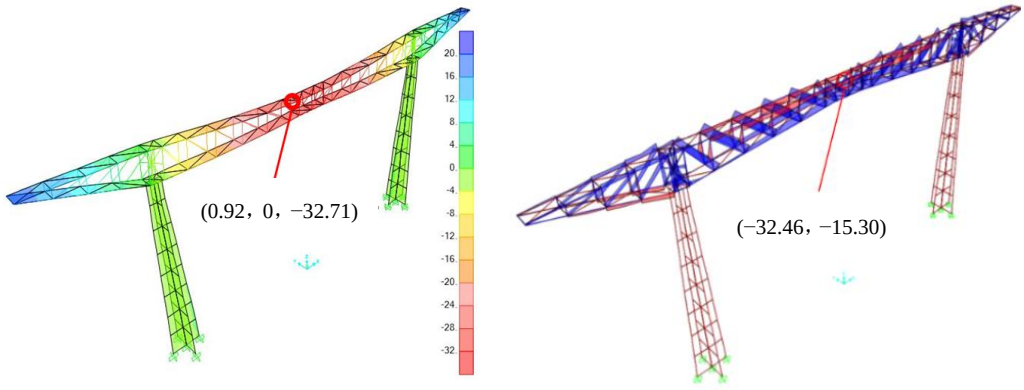

(**a**) (**b**)

Figure 6. Condition 3. (**a**) Deformation pattern. (**b**) Stress diagram.

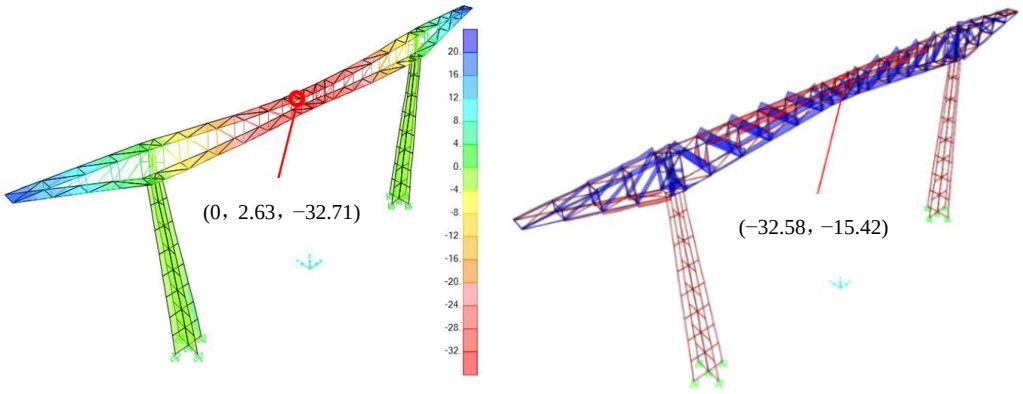

(**a**) (**b**)

Figure 7. Condition 4. (**a**) Deformation pattern. (**b**) Stress diagram.

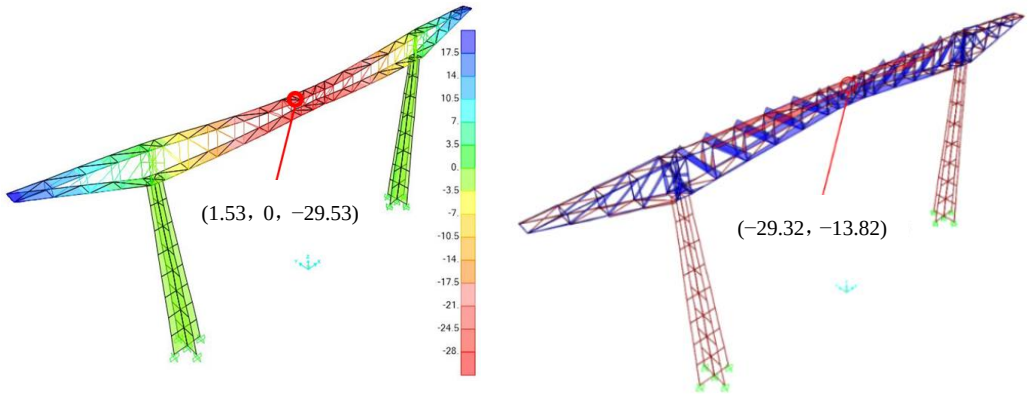

(**a**) (**b**)

Figure 8. Condition 5. (**a**) Deformation pattern. (**b**) Stress diagram.

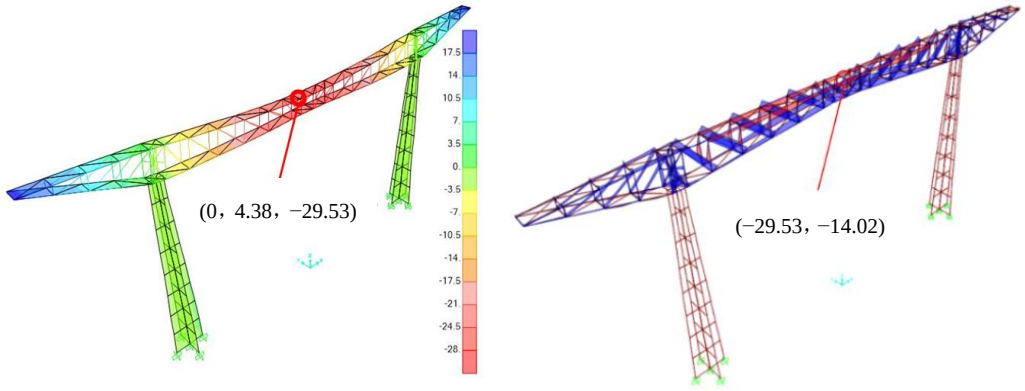

(**a**) (**b**)

Figure 9. Condition 6. (**a**) Deformation pattern. (**b**) Stress diagram.

Table 2. Deformation and stress data for the truss under various conditions.

Load Case	X-Direction Displacement (mm)	Y-Direction Displacement (mm)	Z-Direction Displacement (mm)	Maximum Stress (MPa)	Minimum Stress (MPa)
Condition 1	0	0	−31.78	−31.54	−14.84
Condition 2	0	0	−33.63	−33.36	−15.71
Condition 3	0.92	0	−32.71	−32.46	−15.30
Condition 4	0	2.63	−32.71	−32.58	−15.42
Condition 5	1.53	0	−29.53	−29.32	−13.82
Condition 6	0	4.38	−29.53	−29.53	−14.02

From Figures 4–9 and Table 2, it can be observed that:

(1) With a vertical load, the steel truss of the roof deforms downward across the middle of its span, resulting in the overhanging ends warping upward. The truss displacement in the Z direction is 31.78 mm under condition 1, and the displacement in the Z direction is 33.63 mm under condition 2. Both are within the control range and meet the requirements of the engineering limit of 1/300 span.

(2) Under working conditions 3 and 4, the midspan deformation of the roof steel truss was still vertically downward, with a displacement in the Z direction of 32.71 mm. The displacement in the Z direction was 2.74% less than that for working condition 2, indicating that the wind load does not increase the vertical sag of the structure.

(3) For working conditions 5 and 6, the overhanging area deforms upward. The main truss body deforms by different amounts in the X and Y directions. The deformation in the Z direction is still vertically downward.

(4) Under condition 6, the deformation of the middle part of the roof steel truss meets the limit of 1/300 span, indicating that the structure is always in a safe state no matter what working conditions are encountered during the construction process.

5. Monitoring the Construction Process

The construction process of the eighth steel truss in the landing hall adopts the idea of "bulk transportation + ground assembly + overall hoisting". The construction process is divided into the three following main steps:

(1) Trucks are unloaded using 50 t and 25 t truck cranes, and components are transferred and assembled on the ground.

(2) The assembled truss is lifted by two 250 t crawler cranes.

(3) The truss is hoisted in place, and the hooks are loosened after welding and reinforcement at both ends.

Because there are many monitored steps in the actual construction process, this paper selects the monitoring data from five typical construction nodes, which directly reflect the deformation and stress in the steel truss at each construction stage. The first monitoring is carried out as the truss is hoisted into place. When the welding is completed, most of the members of the steel truss are in compression. The second and third monitoring steps are carried out after the installation of equipment during the construction process. The fourth monitoring step is taken after the roof panel is installed, and the fifth monitoring step is taken after the construction process is basically completed, so there should be no obvious further change in deformation and stress.

5.1. Stress Monitoring

Based on the finite element analysis of the eighth steel truss in the landing hall, the points where critical values of stress and deformation occur are determined, and the monitoring scheme is developed. Each monitored truss has 30 monitored points, distributed at the positions of the top chord, bottom chord, vertical member, and the web member. See Figure 10 for the layout of the points at which stress of the steel structure is measured. The displacement of the pier columns of the substructure is small under the five working conditions. This paper does not consider their changes. The behavior

of the two ends is simplified by viewing them as a fixed hinge support and a sliding hinge support, respectively. The BGK-4000 vibrating-wire-type surface strain gauge is used for stress monitoring. It is connected by a BGK-408 vibrating-wire-type readout (with a built-in temperature sensor). The BGK-4000 vibrating-wire-type surface strain gauge is a strain-measuring instrument installed on the surface of a steel or concrete structure. Its length is 150 mm, its standard measuring range is 3000 με, and its accuracy is ±0.1%. Its full-scale sensitivity is 1.0 με, its working temperature is −20~+80 °C, and it can withstand up to 2.0 MPa of water pressure. The BGK-408 vibrating-wire-type reading instrument is suitable for data acquisition from vibrating-wire-type sensors. The instrument has a fully sealed aluminum-alloy shell, which is suitable for many working environments.

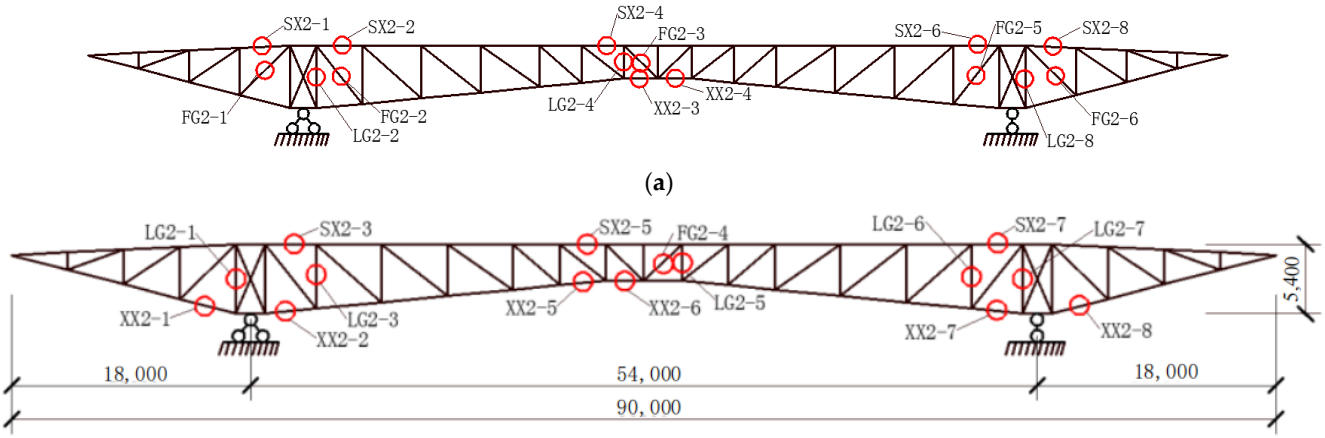

Figure 10. Arrangement of the stress measurement points for (**a**) the view from the north side and (**b**) the view from the south side.

In this paper, 15 representative measuring points were selected for structural stress analysis. When monitoring the stress, we first collect the modulus (R) of each measured point, and then use Equations (1) and (2) to calculate the change in the stress value at this point. The changing stress at each measurement point is shown in Figure 11.

$$\Delta\sigma = \Delta\varepsilon \times E \tag{1}$$

$$\Delta\varepsilon = (R_1 - R_0) \times G \times C \tag{2}$$

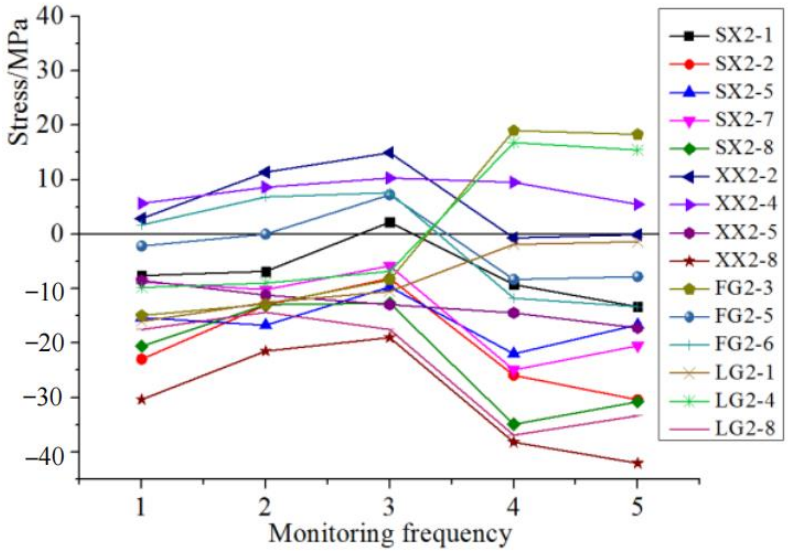

Figure 11. Measured stress curves.

In the formula, $\Delta\sigma$ is the change in the value of the stress (N/mm^2), R_0 and R_1 are the readings of the previous readout and this reading, G is the standard coefficient of the instrument (which is 3.70), and C is the average revision coefficient.

From Figure 11, it can be observed that:

(1) During the construction of a steel truss, its weight is borne by the bearing rod of the support. The members LG2-1 and LG2-8 are located near the bearing rods. The stresses of the members are always negative (in tension) during the construction process. The stress of each member is stable during the final stages of construction. At the last monitoring time, the structural stress of the member LG2-1 is 1.39 MPa, and the structural stress of the member LG2-8 is 33.37 MPa.

(2) The rod XX2-8 is in the lower chord, near the cantilevered end support. During the construction process, its pressure is always greatest. The maximum measured stress value is 42.09 MPa, which should be monitored.

(3) The member XX2-4 is in the middle of the lower chord. Its structural stress varies steadily during the construction process. It always sees small values of tensile stress. The maximum measured value of stress during the construction process is 10.30 MPa. It appears in the middle of the construction period with more staff and equipment.

(4) The maximum measured stress and calculated stress of the member SX2-5 are 21.98 Mpa and 33.36 Mpa, respectively. There are some differences between the measured and calculated stresses. The main reason is that, in the finite element simulation analysis, the conditions influencing the stresses are idealized. This means that the actual structure and the model that is analyzed have some differences, so the simulation results have some discrepancies when compared to the measured values. Although the measured and calculated values are different, they all meet the code requirements, indicating that the construction process is safe.

(5) The unloading has been completed at the fourth data acquisition time. After unloading, all members exhibit sudden changes to different degrees. Most of the forced members are stressed more and more. In the later stage of construction, the stress tends to gradually stabilize.

5.2. Deformation Monitoring

Through the monitored points, the vertical displacements of the key parts of the eighth steel truss in the landing hall of the exhibition center are monitored, such as at the midspan and cantilevered ends of the main truss. The status of the project is monitored during the construction process. The calculated and measured values are compared, and the errors in the construction are analyzed and adjusted. The structural shapes seen during the subsequent construction steps are predicted, and the technical measures to be taken in the subsequent construction steps are put forward. The necessary construction techniques and technical schemes are integrated so that the stress and deformation of the structure after its completion can be effectively controlled, and the quality and safety of the structure can be ensured.

The deformation monitoring points are shown in Figure 12. The layout of the deformation of the monitored points is shown in Figure 13. Firstly, one leveling reference point was selected before the deformation monitoring. The reference point is very steady, and the elevation will not be affected in the construction process. The elevation of the monitored points will be measured in each construction step. The measured vertical displacements are shown in Figure 14.

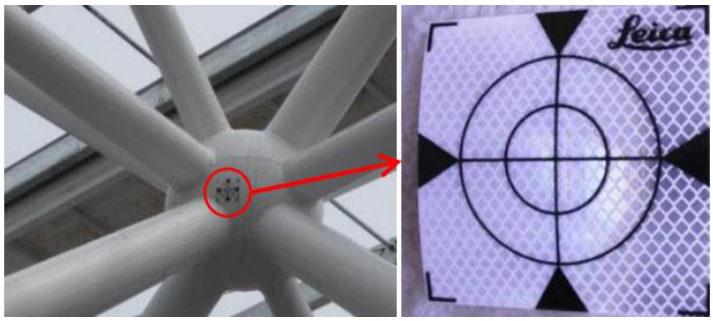

Figure 12. Deformation monitoring points.

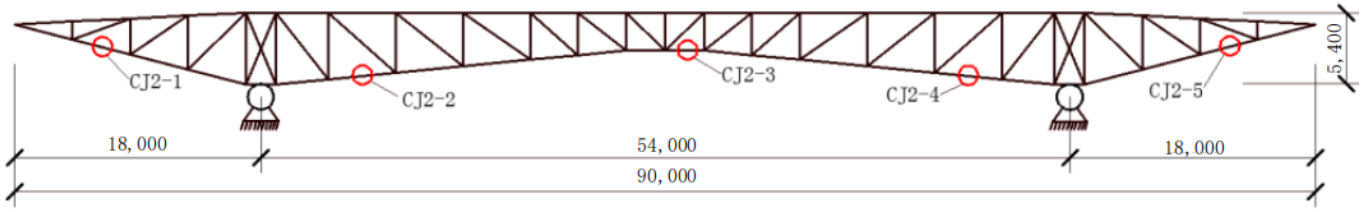

Figure 13. Arrangement of deformation monitoring points.

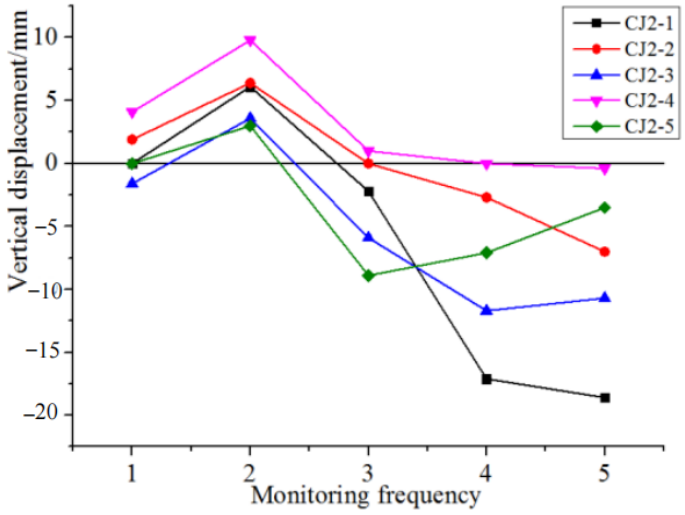

Figure 14. Vertical displacement curves.

From Figure 14, it can be observed that:

(1) During the construction process, the members CJ2-2, CJ2-4, and CJ2-5 are all located in the lower chord near the load-bearing bar. Their measured maximum displacement values are 7.0 mm, 0.4 mm, and 3.5 mm, respectively. The vertical direction is downward, which conforms to the deformation characteristics of the members under uniform loads.

(2) The maximum measured displacement of the member CJ2-1 is 18.6 mm, which is due to the large deformation caused by the heavy loads due to equipment on the roof during splicing, hoisting, and other later construction steps.

(3) The member CJ2-3 is located at the middle of the truss. During the construction process, its vertical direction obviously changes. Its deformation tends to be stable during the later stages of construction. Its maximum measured displacement is 10.7 mm, which meets the requirement that it be less than 1/300 span of the engineering limit value.

(4) The maximum measured value of the deformation of member CJ2-3 in the Z direction is 10.7 mm, and its maximum calculated value is 33.63 mm. The measured and calculated deformation values are basically the same, with the calculated value being

slightly larger than the measured value. The main reason is that the measured value is the measured value for the overlapping section of the roof steel truss of the landing hall, while the calculated value is for the stress state of the eighth steel truss, which is calculated separately. In addition, there are many site factors, such as the impact of imperfect finite element modeling and software, the site and construction environment, construction technology errors, and human measurement errors.

6. Conclusions

(1) The maximum vertical displacement of roof steel truss during different working conditions is 33.63 mm, which meets the requirement that it be less than the engineering limit of 1/300 span. The maximum structural stress is 33.36 MPa, which is within the elastic range of steel.

(2) The maximum measured and calculated stresses of the roof steel truss under different working conditions are 21.98 MPa and 33.36 MPa. The values are far less than the Q345 steel's strength design working strength of 310 MPa.

(3) The method of combining on-site monitoring and simulation analysis can accurately evaluate the structural safety and stability and provide a basis for the subsequent construction and the adjustment of postconstruction monitoring schemes.

Author Contributions: Conceptualization, C.H. and R.H.; methodology, Y.J.; investigation, Y.J. and M.L.; writing—original draft preparation, Y.J.; writing—review and editing, C.H. All authors have read and agreed to the published version of the manuscript.

Funding: This research was funded by the National Natural Science Foundation of China (grant number 52208226) and the Training Plan for Young Key Teachers in Institution of Higher Education in Henan Province (grant number 2019GGJS147).

Institutional Review Board Statement: Not applicable.

Informed Consent Statement: Not applicable.

Data Availability Statement: The data presented in this study are available in the article.

Conflicts of Interest: The authors declare no conflict of interest.

References

1. Zhang, Q.; An, Y.; Zhao, Z.; Fan, F.; Shen, S. Model selection for super-long span mega-latticed structures. *J. Constr. Steel Res.* **2019**, *154*, 1–13. [CrossRef]
2. Su, N.; Peng, S.; Hong, N. Analyzing the background and resonant effects of wind-induced responses on large-span roofs. *J. Wind Eng. Ind. Aerod.* **2018**, *183*, 114–126. [CrossRef]
3. Dong, S.; Zhao, Y.; Xing, D. Application and development of modern long-span space structures in China. *Front. Struct. Civ. Eng.* **2012**, *6*, 224–239. (In Chinese) [CrossRef]
4. Chen, J.; Xiong, J.; Li, G. Acceleration response spectrum for predicting vibrations of long-span structures due to human running load. *Eng. Mech.* **2017**, *34*, 173–181. [CrossRef]
5. Chen, Y.; Zhou, D.; Gui, L. Wind pressure simulation and key influence factors analysis of Mexico-Hat like spatial structures. *J. Vib. Shock.* **2013**, *32*, 37–40. (In Chinese)
6. Li, T.; Yang, Q.; Ishihara, T. Unsteady aerodynamic characteristics of long-span roofs under forced excitation. *J. Wind Eng. Ind. Aerod.* **2018**, *181*, 46–60. [CrossRef]
7. Wang, H.; Zhang, Y.; Mao, J.; Wan, H.; Tao, T.; Zhu, Q. Modeling and forecasting of temperature-induced strain of a long-span bridge using an improved Bayesian dynamic linear model. *Eng. Struct.* **2019**, *192*, 220–232. [CrossRef]
8. Liang, L.; Li, X.; Zheng, J.; Lei, K.; Qin, J. Structure-borne noise from long-span steel truss cable-stayed bridge under damping pad floating slab: Experimental and numerical analysis. *Appl. Acoust.* **2020**, *157*, 106988. [CrossRef]
9. Diana, G.; Fiammenghi, G.; Belloli, M.; Rocchi, D. Wind tunnel tests and numerical approach for long span bridges: The Messina bridge. *J. Wind Eng. Ind. Aerod.* **2013**, *122*, 38–49. [CrossRef]
10. Lee, S.; Yhim, S. Dynamic behavior of long-span box girder bridges subjected to moving loads: Numerical analysis and experimental verification. *Int. J. Solids Struct.* **2005**, *42*, 5021–5035. [CrossRef]
11. Kim, Y.; Park, J.; Oh, B.; Cho, T.; Kim, J.; Kim, S.; Park, H. Practical wireless safety monitoring system of long-span girders subjected to construction loading a building under construction. *Measurement* **2019**, *146*, 524–536. [CrossRef]
12. Chen, Z.; Zong, L.; Ding, Y.; Shi, Y. Improved physical theory model for strut members in long-span spatial structures. *J. Constr. Steel Res.* **2019**, *153*, 85–100. [CrossRef]

13. Feng, B.; Wang, X.; Wu, Z. Fatigue life assessment of FRP cable for long-span cable-stayed bridge. *Compos. Struct.* **2019**, *210*, 159–166. [CrossRef]
14. Santana, M.; Gonçalves, P.; Silveira, R. Stability and load capacity of an elasto-plastic pyramidal truss. *Int. J. Solids Struct.* **2019**, *171*, 158–173. [CrossRef]
15. Feng, L.; Xiong, J.; Yang, L.; Yu, G.; Yang, W.; Wu, L. Shear and bending performance of new type enhanced lattice truss structures. *Int. J. Mech. Sci.* **2017**, *134*, 589–598. [CrossRef]
16. Zhu, Q.; Xu, Y.; Shum, K. Stress-level buffeting analysis of a long-span cable-stayed bridge with a twin-box deck under distributed wind loads. *Eng. Struct.* **2016**, *127*, 416–433. [CrossRef]
17. Mahmoud, Y.; Hassan, M.; Mourad, S.; Sayed, H. Assessment of progressive collapse of steel structures under seismic loads. *Alex. Eng. J.* **2018**, *57*, 3825–3839. [CrossRef]
18. Chen, Z.; Wen, J.; Deng, D.; Dai, W.; Chen, S.; Lu, H.; Liu, L. Research on parametric vibration of a steel truss corridor under pedestrians excitation considering the time-delay effect. *Buildings* **2023**, *13*, 98. [CrossRef]
19. Li, S.; Jiang, W.; Zhu, X.; Xie, X. Effect of localized defects on mechanical and creep properties for pyramidal lattice truss panel structure by analytical, experimental and finite element methods. *Thin-Walled Struct.* **2022**, *170*, 108531. [CrossRef]
20. Li, X.; Pan, J.; Zhou, X. Impact resistance analysis and optimization of variant truss beam structure based on material properties. *Materials* **2021**, *14*, 5847. [CrossRef]
21. Xu, Z.; Zhao, Y.; Deng, C.; Li, Q. Research on seismic isolation of truss string structure with rubber bearings considering relative rotation. *Structure* **2021**, *33*, 1428–1438. [CrossRef]
22. Li, S.; Jiang, W.; Zhu, X.; Xie, X. Experimental and analytical analysis of mechanical properties for large-size lattice truss panel structure including role of connected structure. *Materials* **2021**, *14*, 5099. [CrossRef] [PubMed]
23. Ministry of Construction of the People's Republic of China. *GB 50017-2017*; Code for Design of Steel Structure. China Building Industry Press: Beijing, China, 2017.
24. Ministry of Construction of the People's Republic of China. *GB 50755-2012*; Code for Construction of Steel Structures. China Planning Press: Beijing, China, 2012.
25. Ministry of Construction of the People's Republic of China. *JGJ 257-2012*; Technical Specification for Cable Structures. China Building Industry Press: Beijing, China, 2012.
26. Ministry of Construction of the People's Republic of China. *T/CECS 529-2018*; Early Warning Threshold Standard for Structural Health Monitoring System of Long-Span Bridge. China Building Industry Press: Beijing, China, 2018.
27. Ministry of Construction of the People's Republic of China. *JGJ 7-2010*; Technical Specification for Space Frame Structures. China Building Industry Press: Beijing, China, 2010.